"Bridging Hydroxide Effect" on μ-Carboxylato Coordination and Electrochemical Potentials of Bimetallic Centers: Mn_2(II,II) and Mn_2(III,III) Complexes as Functional Models of Dimanganese Catalases

A. E. M. Boelrijk, S. V. Khangulov, and G. C. Dismukes*

Department of Chemistry, Henry H. Hoyt Laboratory, Princeton University, Princeton, New Jersey, 08540

Received October 5, 1999

Synthesis, solution structures, and electrochemistry of several dinuclear Mn_2(II,II) complexes (**1**−**4**) and Mn_2(III,III) complexes (**6** and **8)**, derived from a functional catalase mimic $[(L^{1,2})Mn_2(II,II)(\mu_{13}\text{-}O_2CCH_3)]^{2+}$ (**1**) are described that enable testing of the role of intramolecular hydroxide ligands on the redox properties. Addition of 1 equiv of hydroxide to **1** or **3** forms $[(L^{1,2})Mn_2(II,II)(\mu_{13}\text{-}O_2CCH_3)(\mu\text{-}OH)]^{+}$ (**7A** or **7B**, respectively), possessing two six-coordinate Mn(II) ions bridged by hydroxide and acetato ligands. Two-electron oxidation of **7** with O_2 occurs by forming $[(L^{1,2})Mn_2(III,III)(\mu_{1,3}\text{-}O_2CCH_3)(\mu\text{-}OH)]^{3+}$ (**8**) and H_2O_2 with no ligand rearrangements in methanol. Reaction of **8** with 2−3 equiv hydroxide forms $[(L^{1,2})Mn_2(III,III)(\mu\text{-}O)(OH)(O_2CCH_3)]^{+}$ in which deprotonation of μ-OH^- to yield μ-O^{2-} favors subsequent addition of a terminal hydroxide ligand, accommodated by a bridging-to-terminal "carboxylate-shift". Preservation of six-coordinate Mn(II) ions throughout all hydroxide-induced transformations is observed, including oxidation by O_2. Cyclic voltammetry reveals that addition of μ-OH^- converts the two-electron redox couple II,II/III,III for complexes **1**−**4** to sequential one-electron couples at lower reduction potentials, yielding substantial stabilization of the II,III and III,III oxidation states by $\Delta E = 440$ and 730 mV, respectively. Binding of a second OH^- to **7A** or **7B** forms $(L^{1,2})Mn_2(II,II)(\mu_{13}\text{-}O_2CCH_3)(OH)_2$, containing two six-coordinate Mn(II) ions with two terminal hydroxides and a $\mu_{1,3}$-bridging acetato. Electrochemistry reveals that displacement of the bridging hydroxide to a terminal site upon addition of the second OH^- restores a two-electron redox couple II,II/III,III but now at a higher reduction potential with considerable loss of the electrochemical stabilization energy provided by the μ-OH^- ($\Delta E = 250$ and 350 mV loss for Mn_2(II,II) and Mn_2(III,III), respectively). These results indicate a considerably stronger influence of bridging vs terminal hydroxide ligands in stabilizing the higher oxidation states and separating the one-electron redox potentials of bimetallic centers. By contrast, in the absence of μ-OH^- bridges the longer separation with the $\mu_{1,3}$-carboxylato bridge in dimanganese-(II,II) complexes leads to nearly complete uncoupling of the Mn(II) oxidation potentials, thus yielding a two-electron redox transition to (III,III). We hypothesize that this "bridging hydroxide effect" may be due to both greater screening of the repulsive intermetallic electric potential energy and increased resonance stabilization of the mixed-valence (II,III) oxidation state by charge delocalization. These data provide a physicochemical basis for interpretation of the catalase activity of these complexes and of dimanganese catalase enzymes (see the following manuscript).

Introduction

Natural methods for protection against H_2O_2 in cells include chemical reduction by cellular reducing agents (ascorbate, glutathione) and catalytic dismutation to form O_2 and H_2O by enzymes called catalases. Understanding the fundamental chemistry of how the dismutation reaction is catalyzed is of considerable current interest because the consequences of unchecked H_2O_2 formation in tissues is considered extremely harmful, being linked to a variety of biochemical oxidations and pathological disorders.[1,21,2] A class of nonheme manganese catalases (MnCAT) has been found from three bacterial origins: *Lactobacillus plantarum* (Lp),[3,4] *Thermus thermophilus* (Tt),[5] and *Thermoleophilum album*[6] with those from *Thermus thermophilus* and *lactobacillus plantarum* being the best characterized. These catalases were shown by various methods including X-ray structure analysis,[7−9] electron paramagnetic resonance,[10] and extended X-ray absorption fine structure (EXAFS) studies[11] to contain a dimanganese center. The *T. thermophilus* catalase contains a $\mu_{1,3}$-carboxylate ligand (glu),

* To whom correspondence should be addressed. E-mail: dismukes@princeton.edu.

(1) Stadtman, E. R.; Berlett, P. B.; Chock, P. B. *Proc. Natl. Acad. Sci. U.S.A.* **1990**, *87*, 384.
(2) Halliwell, B.; Gutteridge, J. M. C. In *Methods of Enzymology*; Packer, L., Glazer, A. N., Eds.; Academic Press: San Diego, 1990.
(3) Kono, Y.; Fridovich, I. *J. Bacteriol.* **1983**, *155*, 742.
(4) Beyer, W. F.; Fridovich, I. *Biochemistry* **1985**, *24*, 6460.
(5) Barynin, V. V.; Grebenko, A. I. *Dokl. Akad. Nauk. SSSR* **1986**, *286*, 461.
(6) Allgood, G. S.; Perry, J. J. *J. Bacteriol.* **1986**, *168*.
(7) Vainshtein, B. K.; Melik-Adamyan, W. R.; Barynin, V. V.; Vagin, A. A.; Grebenko, A. I. *J. Biosci., Proc. Int. Symp. Biomol. Struct. Interact.* **1985**, *8*, 471.
(8) Barynin, V. V.; Vagin, A. A.; Melik-Adamyan, W. R.; Grebenko, A. I.; Khangulov, S. V.; Popov, A. N.; Andrianova, M. E.; Vainshtein, B. K. *Dokl. Akad. Nauk. SSSR* **1986**, *288*, 877 [Russian].
(9) Barynin, V. V.; Hempstead, P. D.; Vagin, A. A.; Antonyuk, S. V.; Melik-Adamyan, W. R.; Lamzin, V. S.; Harrison, P. M.; Artymiuk, P. J. *J. Inorg. Biochem.* **1997**, *67*, 196.
(10) Khangulov, S. V.; Barynin, V. V.; Melik-Adamyan, V. R.; Grebenko, A. I.; Voevodskay, N. V.; Dobrykov, S. N.; Il'ysova, V. B. *Bioorg. Khim.* **1986**, *12*, 741 [Russian].

10.1021/ic9911769 CCC: $19.00
Published on Web 06/17/2000

μ-OH−, and μ-OH_2 as bridges in the reduced Mn_2(II,II) oxidation state, while the Mn_2(III,III) oxidation state contains a μ-oxo bridge in place of the water molecule.[9] These bridges are believed to undergo changes during peroxide dismutation that are critical for catalysis, but their functional significance remains unidentified.

In recent years many dinuclear manganese model complexes have been reported that show catalase activity.[12−33] Still, the best chemical mimics of the dimanganese class of catalases are 10^3−10^5 slower than the enzymes. More effective mimics could find applications in therapies related to treatment of oxidative stress while also elucidating the features important for the enzymatic mechanisms. In those few cases where reaction mechanisms of synthetic mimics have been studied in detail three different types of mechanisms have been found, which differ from one other by the use of different oxidation states in their catalytic cycles. Two types of dimanganese complexes that were examined in detail and that show the involvement of higher (i.e., higher than Mn_2(III,III)) oxidation states are the di-μ-oxosalen complexes, $[Mn^{IV}(salpn)(O)]_2$, and the aminosalen complexes reported by Sakiyama and co-workers,[15,19−21,34−37] which utilize Mn_2(III,III) and Mn_2(IV,IV) states in the catalytic cycle. The latter five-coordinate complexes were shown to form a bismanganyl $(Mn^{IV}{=}O)_2$ species at the end of the peroxide dismutation reaction, which was presumed to be the catalytic species. Studies of several MnCat mimics have revealed that an unsymmetrical coordination of the Mn ions suppresses or eliminates activity.[19,37] Protonation of the bridging oxo in the $[Mn^{IV}(salpn)(O)]_2$ complexes[15,34] was shown to increase the reduction potential[15] and inhibit the catalase activity completely (due to the inability of hydrogen peroxide to oxidize the catalyst to the Mn_2(IV,IV) level), underscoring the importance of ligand protonation and deprotonation for catalytic activity.

complex	L	R	X	Ref.
(1)	L^1	H	H	22
(2)	L^1	H	Cl	22
(3)	L^2	$^{10}CH_2{}^{11}CH_3$	H	this work
(4)	L^2	$^{10}CH_2{}^{11}CH_3$	Cl	this work
(6A)	L^1	H	H	this work
(6B)	L^2	$^{10}CH_2{}^{11}CH_3$	H	this work
(7A)	L^1	H	H	this work
(7B)	L^2	$^{10}CH_2{}^{11}CH_3$	H	this work
(8A)	L^1	H	H	This work
(8A)	L^2	$^{10}CH_2{}^{11}CH_3$	Cl	this work

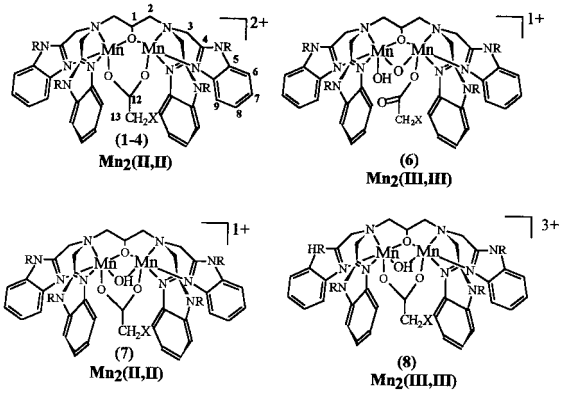

Figure 1. Structures of Mn_2(II,II) complexes, based on the X-ray structures, of crystalline **1** and complexes **1**−**4**, proposed solution structures of a Mn_2(II,II)-μ-OH-$\mu_{1,3}$-acetato complex **7**, and the two kinds of Mn_2(III,III) derivatives (complexes **6** and **8**) obtained after auto-oxidation upon addition of NaOH (see text and Scheme 3 for details). "#A" indicates a species derived from chelate L^1, "#B" indicates a species coming from chelate L^2.

So far only two functional model systems have been reported that use the low-valent Mn_2(II,II) ↔ Mn_2(III,III) cycle similar to those of the enzymes. By a modification of the H_2salpn ligand to yield a 2-hydroxypropane backbone, Pecoraro et al. obtained a series of dimanganese complexes, $Mn_2(salpn{-}O)_2X$, in which two μ-alkoxide anions serve to bridge the Mn_2(II,II) and Mn_2(III,III) ions.[13,23,33,38−40] The first functional catalase model complex employed a septadentate ligand (Figure 1).[14] Improved catalase rates and enhanced stability were found upon replacement of terminal halide ligands by a $\mu_{1,3}$-carboxylato.[12,41] The solid-state structures of the latter derivatives show a coordinated solvent molecule leading to five- and six- coordinated Mn(II) ions (Figure 1, structures **1** and **2**).

Herein, we report solution-phase spectroscopic studies of two Mn_2(II,II) complexes and their oxidized Mn_2(III,III) complexes, including new ligand derivatives that contain *N*-alkylated benzimidazoles. The solution structures and redox properties of these new species and their interconversion with less active species were studied by optical, infrared, electron paramagnetic

(11) Waldo, G. S.; Yu, S.; Penner-Hahn, J. E. *J. Am. Chem. Soc.* **1992**, *114*, 5869.
(12) Pessiki, P. J.; Dismukes, G. C. *J. Am. Chem. Soc.* **1994**, *116*, 898.
(13) Gelasco, A.; Pecoraro, V. L. *J. Am. Chem. Soc.* **1993**, *115*, 7928.
(14) Mathur, P.; Crowder, M.; Dismukes, G. C. *J. Am. Chem. Soc.* **1987**, *109*, 5227.
(15) Larson, E. J.; Pecoraro, V. L. *J. Am. Chem. Soc.* **1991**, *113*, 7809.
(16) Larson, B.; Lah, M. S.; Li, X.; Bonadies, J. A.; Pecoraro, V. L. *Inorg. Chem.* **1992**, *31*, 373.
(17) Bossek, U.; Saher, M.; Weyhermuller, T.; Wieghardt, K. *J. Chem. Soc., Chem. Commun.* **1992**, 1780.
(18) Sarneski, J. E.; Brzezinski, L. J.; Anderson, B.; Didiuk, M.; Manchanda, R.; Crabtree, R. H.; Brudvig, G. W.; Schulte, G. K. *Inorg. Chem.* **1993**, *32*, 3265.
(19) Sakiyama, H.; Tamaki, H.; Kodera, M.; Matsumoto, N.; Okawa, H. *J. Chem. Soc., Dalton Trans.* **1993**, 591.
(20) Sakiyama, H.; Okawa, H.; Isobe, R. *J. Chem. Soc., Chem Commun.* **1993**, 882.
(21) Sakiyama, H.; Okawa, H.; Suzuki, M. *J. Chem. Soc., Dalton Trans.* **1993**, 3823.
(22) Pessiki, P. J.; Khangulov, S. V.; Ho, D. M.; Dismukes, G. C. *J. Am. Chem. Soc.* **1994**, *116*, 891.
(23) Pecoraro, V. L.; Baldwin, M. J.; Gelasco, A. *Chem. Rev.* **1994**, *94*, 807.
(24) Gelasco, A.; Askenas, A.; Pecoraro, V. L. *Inorg. Chem.* **1996**, *35*, 1419.
(25) Nagata, T.; Mizukami, J. *J. Chem. Soc., Dalton Trans.* **1995**, 2825.
(26) Naruta, Y.; Maruyama, K. *J. Am. Chem. Soc.* **1991**, *113*, 3595.
(27) Naruta, Y.; Sasayama, M. *J. Chem. Soc., Chem. Commun.* **1994**, 2667.
(28) Naruta, Y.; Sasayama, M. *Angew. Chem., Int. Ed. Engl.* **1994**, *33*, 1839.
(29) Devereux, M.; Curran, M.; McCann, M.; Casey, M. T.; McKee, V. *Polyhedron* **1995**, *14*, 2247.
(30) Devereux, M.; Curran, M.; McCann, M.; Casey, M. T.; McKee, V. *Polyhedron* **1996**, *15*, 2029.
(31) Nishida, Y.; Nasu, M. *Inorg. Chim. Acta* **1991**, *190*, 1.
(32) Nishida, Y.; Akamatsu, T.; Tsuchiya, K.; Sakamoto, M. *Polyhedron* **1994**, *13*, 2251.
(33) Gelasco, A.; Bensiek, S.; Pecoraro, V. L. *Inorg. Chem.* **1998**, *37*, 3301.
(34) Larson, E. J.; Pecoraro, V. L. *J. Am. Chem. Soc.* **1991**, *113*, 3810.
(35) Itoh, M.; Motoda, K.; Kamiusuli, T.; Sakiyama, H.; Matsumo, N.; Okawa, H. *J. Chem. Soc., Dalton Trans.* **1995**, 3635.
(36) Higuchi, C.; Sakiyama, H.; Okawa, H.; Fenton, D. E. *J. Chem. Soc., Chem. Commun.* **1995**, 4015.
(37) Wada, H.; Motoda, K.; Ohba, M.; Sakiyama, H.; Matsumoto, N.; Okawa, H. *Bull. Chem. Soc. Jpn.* **1995**, *68*, 1105.
(38) Gamelin, D. R.; Kirk, M. L.; Stemmler, T. L.; Pal, S.; Armstrong, W. H.; Penner-Hahn, J. E.; Solomon, E. I. *J. Am. Chem. Soc.* **1994**, *116*, 2392.
(39) Gelasco, A.; Kirk, M. L.; Kampf, J. W.; Pecoraro, V. L. *Inorg. Chem.* **1997**, *36*, 1829.
(40) Pecoraro, V. L.; Gelasco, A.; Baldwin, M. J. *Modeling the chemistry and properties of multinuclear manganese centers*; Kessissoglou, D. P., Ed.; Kluwer Academic Publishers: The Netherlands, 1995; p 287.
(41) Pessiki, P. J. *An Investigation of Synthetic Complexes that Model the Dinuclear Manganese Catalases and the Iron−Histidine−Quinone Complex of Photosystem II*. Ph.D. Thesis, Princeton University Press: Princeton, NJ, 1994.

resonance (EPR), and paramagnetic NMR spectroscopies, mass spectrometry, and cyclic voltammetry. These data are used to identify the catalytic intermediates in the disproportionation of hydrogen peroxide, which is described in the following manuscript.[42]

Experimental Section

Synthesis. All solvents were of HPLC grade and used without further purification unless stated otherwise. 2,6-Di(tertbutyl)pyridine (TBP) was commercially available from Aldrich and was used without purification. $[L^1Mn_2(CH_3CO_2)](ClO_4)_2$ (**1**) and $[L^1Mn_2(ClCH_2CO_2)](ClO_4)_2$ (**2**), where L^1 is *N*,*N*,*N*′,*N*′-tetrakis(2-methylenebenzamidazolyl)-1,3-diaminopropan-2-ol, were synthesized as described previously.[22] *N*,*N*,*N*′,*N*′-tetrakis(2-(1-ethylbenzamidazolyl))-2-hydroxy-1,3-diaminopropane (L^2) was synthesized according to the procedure of McKee et al.[43] The dimanganese (II,II) complexes $[L^2Mn_2(CH_3CO_2)](ClO_4)_2$ (**3**) and $[L^2Mn_2(ClCH_2CO_2)](ClO_4)_2$ (**4**) were prepared following the procedures for **1** and **2** and isolated as white crystalline solids and did not need to be further purified. In the abbreviation of the molecular formulas "A" indicates complexes with L^1 while "B" indicates complexes with L^2.

Complex **3**, spectral data: FT-IR (KBr, cm^{-1}), $\mu_{1,3}$-carboxylate 1564 (unsymmetrical) and 1433 (symmetrical), 1490 and 1450 benzimidazole ring C═N−C stretching, 1085 perchlorate. Mass spectrometry (electrospray), MW 989 corresponding to the monocation $\{[L^2Mn_2(CH_3CO_2)](ClO_4)\}^{1+}$.

Complex 4, spectral data: FT-IR (KBr, cm^{-1}), $\mu_{1,3}$-carboxylate 1592 (unsymmetrical) and 1405 (symmetrical), 1491 and 1452 benzimidazole ring C═N−C stretching, 1090 perchlorate. Mass spectrometry (electrospray), MW 1024 corresponding to the monocation $\{[L^2Mn_2(CH2ClCO2)](ClO_4)\}^{1+}$.

Optical Absorption. All studies in the range 200−800 nm were carried out using a Hewlett-Packard model 8450 spectrophotometer. All solvents were of spectroscopic grade and dried over molecular sieves prior to use. A quartz cell with a path length of 1 cm was used in all experiments. Sodium hydroxide was added as a 2×10^{-3} M solution in methanol.

Electrochemistry. The cyclic voltammetry experiments were performed with a model 363 potentiostat in line with a Cypress Systems, CYSY model 1, computer-controlled electroanalysis system or a computer-controlled Princeton Applied Research potentiostat, model 270, with model 270/250 Research Electrochemistry Software. In all experiments a single compartment cell with a three-electrode configuration was used: glassy carbon (working electrode)/platinum (counter electrode)/SCE (reference electrode). All solutions were 1 mM in complex and 1 M in $(n\text{-butyl})_4NClO_4$ (TBAP) in acetonitrile or acetone, which was previously dried over molecular sieves. The solutions were thoroughly degassed with argon prior to experiments, and all voltammetric measurements were done under a positive pressure of this gas. To allow comparison with the literature data, we point out that under our experimental conditions $E_{1/2}^{ref}$ for the couple (biscyclopentadienyl)-Fe(II)/Fe(III) was 0.375 V vs SCE in acetonitrile and acetone. The $E_{1/2}$ values in this work were computed from cyclic voltammetric wave forms as the half-sum of anodic and cathodic peak potentials. From each waveform the appropriate baseline, due to the acetonitrile/TBAP or acetone/TBAP solution, was subtracted.

NMR Spectroscopy. ^1H NMR spectra of the model complexes were obtained on a GE QE-300 MHz spectrometer at room temperature. Reported spectra of 10 mM samples were accumulated over a 50 kHz bandwidth for each sample. Chemical shifts were referenced to TMS or resonances due to residual protons present in the deuterated solvent. NaOD solutions were prepared by diluting a 40% NaOD/D_2O solution in deuterated methanol. DCl solutions were prepared by diluting a 20% DCl/D_2O solution with deuterated methanol.

FT Infrared Studies. All IR samples were run as KBr pellets in the range 4000−600 cm^{-1} on a Nicolet 730 FTIR spectrometer collecting 32 scans on average.

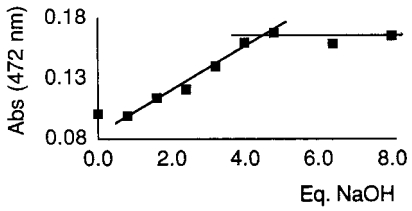

Figure 2. Titration showing the formation of the absorption band at 472 nm for complex **8A** upon addition of 0−8 equiv of NaOH to complex **1** under O_2-saturated conditions in methanol solvent.

EPR. Spectra at 9.43 GHz were obtained with a Bruker ESP-300 spectrometer in the temperature range 4.2−77 K using an Oxford Instruments helium cryostat. All samples were 1 mM in concentration.

Mass Spectrometry. A Kratos MS 50 mass spectrometer was used for fast-atom bombardment (FAB) measurements using thioglycerol or nitrobenzyl alcohol as a matrix. A Hewlett-Packard 5989B MS engine was used for electrospray measurements in the positive mode using methanol as a solvent.

Results

Auto-oxidation of Complexes 1−4. Under argon gas, the methanolic solutions containing complexes **1**−**4** remain colorless upon the addition of hydroxide. However, the same reactions run under air produces an orange solution that reaches an absorption end point after 5 equiv of NaOH, as monitored by UV−vis absorption. Figure 2 shows the increase of the absorption band at 472 nm upon addition of 0−8 equiv Of NaOH to **1** under O_2-saturated conditions in methanol solvent. The visible spectrum of the orange species obtained at the end point of this titration is included in the Supporting Information (Figure S1). This spectrum is identical to the spectrum of the reaction product obtained upon reaction of complex **1** with a stoichiometric amount of H_2O_2 in methanol, which was reported before.[12] Both spectra reveal three absorption peaks at 425, 472, and 760 nm, which were previously assigned to oxidation to a Mn(III) or Mn_2(III,III) species on the basis of their absence in the initial Mn_2(II,II) species. These bands are consistent with Mn(III) ligand field transitions in a low symmetry environment or possibly ligand-to-Mn(III) charge-transfer transitions.[38] The oxidation of **1** cannot be reversed by bubbling with argon gas nor is any dioxygen released. Complex **3** with N-alkylated benzamidazoyls shows identical oxidation chemistry upon addition of NaOH, i.e., formation of an identical electronic spectrum with absorptions at 425, 472, and 760 nm. Hence, we conclude that the Mn oxidation reaction with NaOH and air does not involve deprotonation of the benzimidazole groups. Isolation of the oxidized species in a microcrystalline form was performed by precipitation by dropwise addition of diethyl ether. However, isolation of either of these species as a single crystal suitable for X-ray diffraction has not been successful so far.

EPR Spectroscopy. The similarity between the EPR signals for complex **1** and $MnCat^{II,II}$ from *T. thermophilus* was reported before.[12] Both spectra are centered at $g = 2.0$ and exhibit ^{55}Mn hyperfine and zero-field splittings typical of antiferromagnetically spin-coupled Mn_2(II,II) centers possessing an even-spin electronic state origin (both the $S = 1$ and $S = 2$ states are observable). Addition of an excess of hydrogen peroxide significantly bleaches the EPR signal, consistent with formation of a Mn(III) or Mn_2(III,III) species, as is also evident from the optical absorption change (discussed above). By lowering of the temperature (<10 K) and the microwave power used for detection of the EPR spectra, it is possible to selectively detect the presence of Mn(II) centers, even in the presence of much larger concentrations of a spin-coupled Mn_2(II,II) center. The

(42) Boelrijk, A. E. M.; Dismukes, G. C. Inorg. Chem. **2000**, *39*, 3020.
(43) McKee, V.; Zvagulis, M.; Dagdigian, J. V.; Patch, M. G.; Reed, C. A. *J. Am. Chem. Soc.* **1984**, *106*, 4765.

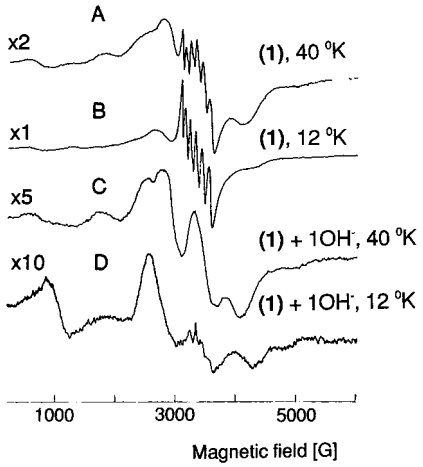

Figure 3. Temperature dependence of the EPR spectra of complex **1** in 95%MeOH/5% H_2O at 40 K (A) and 12 K (B) and after addition of 1 equiv of NaOH under anaerobic conditions to complex **1**, yielding complex **7A**, measured at 40 K (C) and 12 K (D).

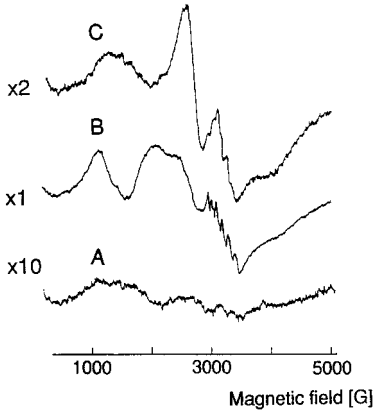

Figure 4. EPR spectra of complex **1** measured at 10 K: (A) in dry acetone, indistinguishable from baseline; (B) in 95% acetone/5% H_2O forming either complex **5A** or **5B**; (C) upon addition of 1 equiv of NaOH to the solution in (B), yielding complex **7A**.

spin-coupled complex **1** has an energy splitting of 23 cm^{-1} between the ground singlet and excited triplet states and so is diamagnetic and EPR-silent at temperatures below 10 K,[44] while a spin-uncoupled Mn_2(II,II) center has an EPR signal with a Curie temperature dependence (proportional to T^{-1}) in the range from 10 to 50 K. This approach was used to separately identify spectra from both spin-coupled and spin-uncoupled Mn_2(II,II) complexes produced as described next.

In dry acetone the EPR spectrum of the excited triplet and higher spin states of complex **1** can be observed only at relatively high temperature (>40 K) because of the energy splitting. The spectrum is characteristic of a well-studied class of spin-coupled dinuclear Mn_2(II,II) species[10,14,22,44] and could be assigned to an axially distorted complex having a zero-field splitting value (D) estimated to be between 0.56 and 0.70 cm^{-1} based on the high-field transition of the $S = 2$ quintet state (Supporting Information, Figure S1).[44] No signals due to a spin-uncoupled Mn(II) (mononuclear) species are observed at any temperature in dry acetone solvent (for example, 10 K, Figure 4A).

However, following addition of small amounts of water (1−5%) to an acetone solution of complex **1,** a six-line Mn(II) EPR signal appears at $g = 2$ accompanied by a broad low-field peak at 1100−1600 G (Figure 4B). The yield is estimated to be 20% based on the concentration of **1**. These signals both exhibit a Curie temperature dependence (not shown) and can be attributed to a mononuclear Mn(II) or spin-uncoupled dinuclear Mn(II) species. The isolated spectra for the spin-coupled and the spin-uncoupled Mn_2(II,II) species were obtained by deconvolution of the temperature-dependent spectra over the range 10−50 K using standard multicomponent analysis methods.[44] The resulting isolated spectra agree completely with the original complex **1** and the spin-uncoupled Mn_2(II,II) spectra described above (deconvoluted spectra given in Supporting Information, Figures S1 and S2). The six-line signal is attributed to an uncoupled dinuclear Mn_2(II,II) complex based on (1) the presence of the six-line ^{55}Mn hyperfine splitting at $g = 2$, (2) its Curie temperature dependence, (3) the fact that the yield increases upon addition of water, and (4) that complete conversion of the coupled Mn_2(II,II) species into the spin-uncoupled derivative can be observed upon addition of 1 equiv of acid ($HClO_4$). Upon subsequent addition of 1 equiv of NaOH to this solution (spectra C and D of Figure 3), the spin-coupled (majority) species increases in yield while the spin-uncoupled species disappears again, suggesting that deprotonation of the alcohol function of L^1H restores electronic coupling of the Mn(II) ions and regenerates the spin-coupled EPR signal. Addition of more equivalents of NaOH to this solution causes no further change in the absence of air. However, in the presence of air the oxidized Mn_2(III,III) orange species appears (as described above) and the spin-coupled Mn_2(II,II) EPR signal decreases in parallel, consistent with the transformation to a Mn(III) monomer or Mn_2-(III,III) species.

From these EPR spectra we conclude that the alkoxide moiety of the ligand that bridges the two manganese ions in complexes **1**−**4** can be reversibly protonated and deprotonated when water is present in solution. Consequently, this process needs to be considered also during the reaction with hydrogen peroxide (see the following manuscript). These conversions are summarized in step A of Scheme 3 where formation of a spin-uncoupled

Scheme 1. Free Energy Diagram Depicting the Electrochemical Conversions of Complex **1** and upon Addition of Hydroxide

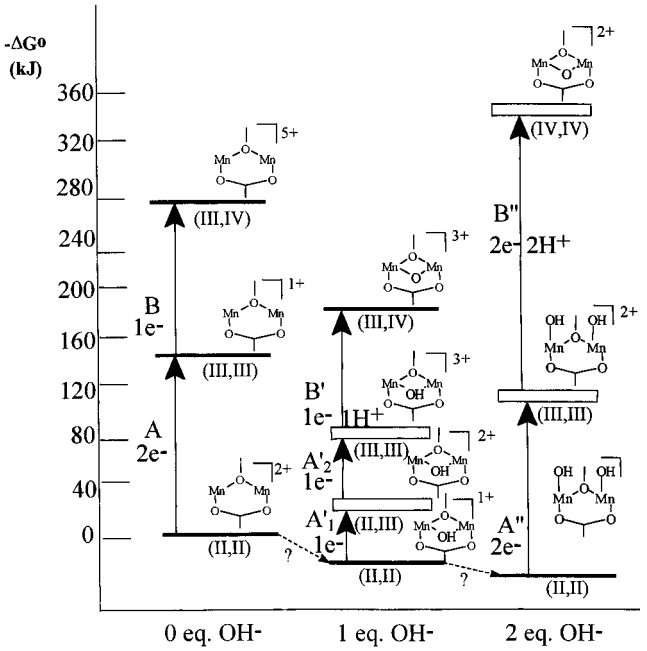

(44) Khangulov, S. V.; Pessiki, P. J.; Barynin, V. V.; Ash, D.; Dismukes, G. C. *Biochemistry* **1995**, *34*, 2015.

Scheme 2. Free Energy Diagram Depicting the Electrochemical Conversions of Complex **1** upon Removal of One and Two Protons from the Benzamiidazoyl Groups of the Ligand, L^1-H and L^1-2H, Respectively, by Addition of 2,6-Di(t-butyl)pyridine (TBP)[a]

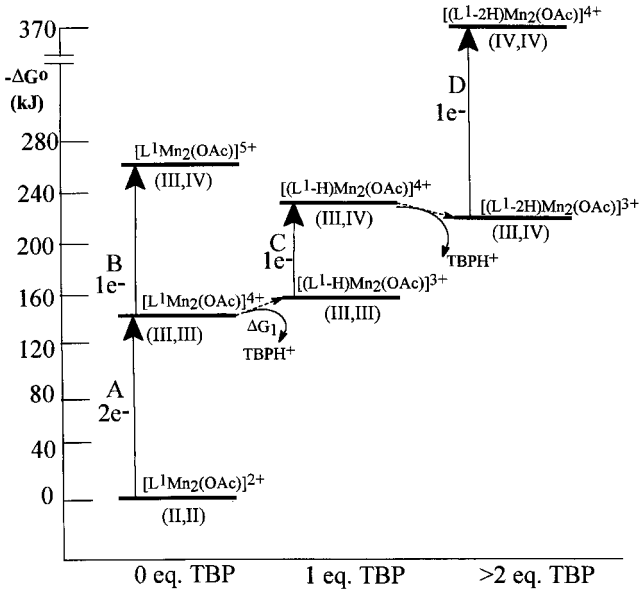

[a] The value for ΔG_1 is estimated to have a lower limit of 14 kJ based on the pK_a of TBP.

Mn_2(II,II) center is proposed via protonation of the alkoxo bridge, resulting in a loss of one Mn−alkoxide bond. From the EPR data alone one cannot deduce whether the μ-acetate remains coordinated. Therefore, both structures **5A** and **5A′** are feasible (see step A, Scheme 3).

^{1}H NMR Spectroscopy. High-spin Mn(III) and Mn_2(III,III) complexes typically show well-resolved isotropically shifted ^{1}H NMR spectra arising from ligand protons.[45] The spectra of a number of Mn_2(III,III) complexes indicate that the size of the isotropic shift of the protons reflects the strength of the intermanganese antiferromagnetic coupling interaction,[15,34,46,4746,47] as was shown before for diiron complexes.[48]

Complex **8**, the orange Mn_2(III,III) product of complex **3** obtained by air oxidation in NaOH (see steps B and C of Scheme 3), is highly soluble in acetone and methanol, unlike complex **3** itself, which is only sparingly soluble ($<10^{-4}$ M). We took advantage of the insolubility of complex **3** to obtain the ^{1}H NMR spectrum and yield of complex **8B** by filtration to remove unreacted complex **3**. Upon titration of a solution of the Mn_2(II,II) complex **3** with 1−4 equiv of NaOD in deuterated methanol and filtration of the sample, several sharp resonances appear in the 0−10 ppm region of the ^{1}H NMR spectrum and one broad resonance at 22.8 ppm. Parts A, B, and C of Figure 5 illustrate the changes compared to the spectrum of complex **8B** upon addition of 1, 2, and 4 equiv of NaOD, respectively. The resonance positions of the spectrum of complex **8B**, their integral areas and line widths, and a tentative assignment are tabulated in Table 1. The full NMR spectrum of complex **8B** is available in the Supporting Information. The small paramagnetic shifts of the ligand protons indicate the presence of strong antiferromagnetic coupling between the Mn ions in the Mn_2(III,III) species. Figure 5B reveals that titration with NaOH eliminates the broad resonance located at 22.8 ppm between 2 and 4 equiv of NaOH. The disappearance of this signal coincides with the appearance of a new signal at 1.90 ppm, as shown in Figure 5A. Figure 5C shows the relation between the integration area of the 1.9 ppm resonance and the 22.8 ppm resonance. The other signals assigned to the macrocyclic ligand remain unchanged (Table 1). The signal at 22.8 ppm is assigned to the methyl group of the bridging acetate on the basis of its integration and its large downfield shift, analogous to other Mn_2(III,III) μ-acetato complexes.[49] On the basis of these NMR spectra, two simultaneous structural rearrangements are observed to occur upon addition of OH^-. We assign these to conversion

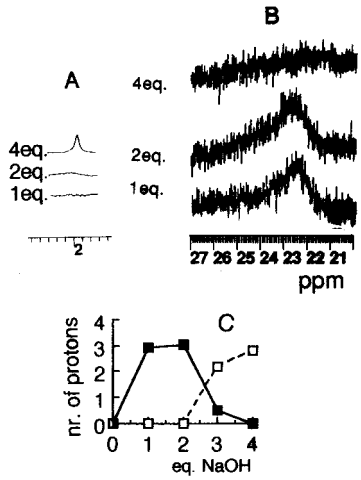

Figure 5. ^{1}H NMR spectrum. Parts A and B show the increase of signal at 1.9 ppm and decrease of the broad signal at 22.8 ppm, respectively, upon addition of 1−4 equiv of NaOD to a solution of complex **8B** in MeOD (see text and Table 1 for details and assignments). Part C shows the relation between the integration area of the 1.9 ppm resonance (□) and the 22.8 ppm resonance (■).

Table 1. Summary of NMR Data for the Mn_2(III,III) Auto-oxidation Derivatives **6B** and **6′B**, Obtained from Complexes **3** and **4**, Respectively (See Figure 5)

assignment[c]	chem shift complex **6B** and complex **6′B** in parentheses (ppm vs TMS)	area (protons)	line width (Hz)
H_{11}	0.98 (0.95)	12	20
H_{13} (monodentate acetate)	1.90[a,b]	2.8	24
H_2	2.54 (2.52)	4	33
MeOH	3.31 (3.29)		13
H_1	3.64 (3.60)	1	24
H_3	3.90 (3.89)	8	23
H_{10}	3.99 (4.00)	8	23
water	4.90 (4.96)		10
H_{5-9}	7.25−7.56 (7.25−7.68)	16	17

[a] The CH_2 resonance of monodentate-coordinated $ClCH_2COO^-$ is hidden under the water signal at 4.96 ppm. [b] The CH_3 and CH_2Cl resonacnes of bidentate-coordinated CH_3COO^- and $ClCH_2COO^-$, respectively, are not present in complex **6** obtained after addition of 3 equiv or more of NaOD but are present in **8** obtained for 2 equiv or fewer of NaOD. See discussion section and inset of Figure 5 for details. [c] For numbering of positions see Figure 1.

(45) Bertini, I.; Luchinat, C. *NMR of paramagnetic molecules in biological systems*; Benjamin/Cummings Publishing Company: Menlo Park, CA, 1986.
(46) Bonadies, J. A.; Kirk, M. L.; Lah, M. S.; Kessissoglou, D. P.; Hatfield, W. E.; Pecoraro, V. L. *Inorg. Chem.* **1989**, *28*, 2037.
(47) Bonadies, J. A.; Maroney, M. J.; Pecoraro, V. L. *Inorg. Chem.* **1989**, *28*, 2044.
(48) Maroney, M. J.; Kurtz, D. M.; Nocek, J. M.; Pearce, L. L.; Que, L., Jr. *J. Am. Chem. Soc.* **1986**, *108*, 6871.
(49) Sheats, J. E.; Czernuziewicz, R.; Dismukes, G. C.; Rheingold, A.; Petrouleas, V.; Stubbe, J.; Armstrong, W. H.; Beer, R.; Lippard, S. J. *J. Am. Chem. Soc.* **1987**, *109*, 1435.

Scheme 3. Interconversions of the Parent Mn_2(II,II) Complexes **1**−**4** upon Addition of Hydroxide in Acetone[a]

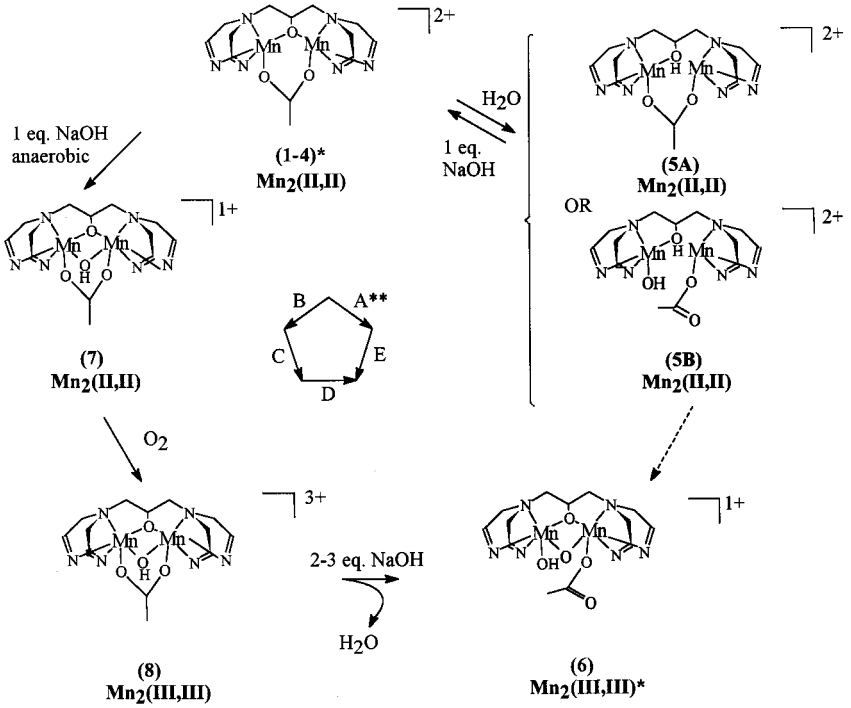

[a] Step A is less than 20% in water. ∗ denotes stable solid. ∗∗ denotes that the conversion in step A is less than 20%. See text for details.

of the $\mu_{1,3}$-bridging acetate to a labile monodentate terminal site that appears to be in equilibrium with free acetate (Scheme 3, step D). Because of the large line width (J = 24 Hz) of the new 1.90 ppm resonance, it is unlikely that acetate is completely removed from the dimanganese core. Indeed, upon addition of excess sodium acetate to this solution, a much sharper resonance (J = 14 Hz) signal appears for free acetate in the spectrum at 1.89 ppm.

The reversibility of the conversion between Mn_2(II,II) and Mn_2(III,III) was proven by successive addition of 2 equiv of NaOD to complex **3** in air-saturated methanol followed by 2 equiv of DCl. This treatment causes all ^{1}H NMR resonances to first appear during oxidation and then to disappear in DCl concomitant with the solution becoming colorless and some white solid **3** precipitating. The identity of the reducing agent responsible for the autoreduction in DCl was not investigated, although it is assumed that it is H_2O_2 that was previously formed from O_2 in the oxidation reaction of complex **3** under basic conditions. Upon addition of another 2 equiv of NaOD to this colorless suspension, the orange color returns, the complex resolubilizes again, and the NMR spectrum shows the reappearance of the original resonances of the Mn_2(III,III) complex. Only a minor destruction of the complex occurs, indicated by the appearance of extra signals (Supporting Information, Figure S3).

Complex **4**, which has a coordinated $\mu_{1,3}$-chloroacetate instead of $\mu_{1,3}$-acetate, shows identical chemistry upon addition of 1−4 equiv of NaOD, including loss of a broad ^{1}H NMR signal around 22.8 ppm at and above 3 equiv of NaOD (Table 1). However, positive identification of the formation of the monodentate-coordinated chloroacetate could not be confirmed because the expected signal is very close to that for free chloroacetate, which is hidden under a solvent peak in the spectrum.

In contrast to complex **3**, complex **1**, $[L^1Mn_2(CH_3CO_2)](ClO_4)_2$, is very soluble in methanol and acetone.[12] Also in this case an orange solution is formed upon addition of NaOD under air. However, the NMR spectra are of poorer quality than with

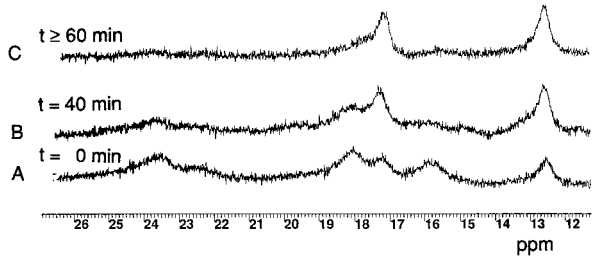

Figure 6. ^{1}H NMR spectra of **8A**, the oxidized Mn_2(III,III) derivative of complex **1** in MeOD, obtained upon addition of 3 equiv of NaOD at t = 0 min (A), 40 min (B), and 60 min or greater (C).

complex **3** because of additional line-broadening. The spectrum of **1** after addition of 3 equiv of NaOD shows broad signals between −2 and 10 ppm, which are poorly resolved and are difficult to assign to specific protons (Supporting Information, Figure S4). Since complex **1** is readily soluble in methanol, it cannot be removed by filtration, and thus, unoxidized material remains in the solution and causes further line-broadening. Alternatively, the broadening may be due to proton exchange with the benzimidazole groups in L^1, which could effect the paramagnetic shift of all ^{1}H resonances through modulation of the Mn(III) exchange coupling. Addition of more NaOD did not further change these resonances or improve the quality of the spectrum. Qualitatively, the spectral changes suggest that the same interconversions appear to occur for both complexes **1** and **3**.

An extra feature of the ^{1}H NMR spectrum of the Mn_2(III,III) derivative of **1** that is not observed in the spectra of the Mn_2-(III,III) derivative of complex **3** is the presence of six broad signals in the 12−25 ppm region following addition of 3 equiv of NaOH (Figure 6A). These signals are due to the D_2O exchangeable protons on the benzimidazole nitrogens, which must be absent in the oxidized derivative of complex **3**, since the benzimidazole nitrogens are alkylated in this complex. The existence of six different N−H signals suggests the presence of several species. However, when the sample is left for 40 min

(Figure 6B) and 1 h or longer (Figure 6C) at room temperature, this spectrum simplifies in the 10−30 ppm region and only two N−H signals at 13 and 17.5 ppm remain while there is no change in the 10 to −2 region (not shown). Integration of the 10−30 ppm area shows that the overall number of N−H protons remains constant during this transformation, i.e., the initial species that shows six peaks for the six NH protons (four benziimidazoyls and two tertiary amines) is converted to the species that gives rise to only two resolved NH signals. The simplified spectrum is expected from a symmetric (μ-O)−(μ-OR)Mn_2(III,III) dimer in which only two magnetically different NH groups are present. We propose that one pair of N−H's belongs to the benzimidazole groups coordinated trans to the μ-alkoxide bridge and that the other pair of N−H's belongs to the benzimidazole groups coordinated trans to the μ-oxo group. The fact that the final spectrum after reaching equilibrium in air does not contain a $\mu_{1,3}$-acetate signal at 22.8 ppm indicates that the symmetrical ($\mu_{1,3}$) acetate bridge is broken following air oxidation in base, a reaction that is analogous to the behavior of complex **3**. Complex **2** differs from complex **(1** only by replacing acetate by a chloroacetate bridge and shows the same chemistry upon addition of NaOD as complex **1**. The chemical reactions that take place upon addition of NaOH to complexes **1**−**4** are summarized in steps B, C, and D of Scheme 3.

FTIR Measurements. The Mn_2(III,III) derivatives formed by air oxidation of complexes **1**−**4** all precipitate from the methanol/NaOH solutions in 1−2 days as amorphous solids. So far we have not been able to obtain crystalline material suitable for single-crystal X-ray structural analysis. Hence, FTIR spectra were obtained to determine the stereochemistry of the coordination of the carboxylate group.[50] An analysis of the FTIR spectrum of complex **1** was reported before[12] and shows two modes at 1564 and 1427 cm^{-1} for the asymmetric and symmetric stretch mode of a symmetrical $\mu_{1,3}$-bridging acetate ($\Delta\upsilon$ = 137 cm^{-1}). In the FTIR spectrum of the precipitated Mn_2(III,III) derivative of complex **1**, the asymmetric stretch at 1564 cm^{-1} disappears and a new strong mode appears at 1627 cm^{-1}. This new absorption indicates a monodentate coordination of acetate, since the increase of the υ_{asym} stretch by 63 cm^{-1} supports formation of the pseudo-ester configuration (Mn−O−C(=O)CH_3).[50] The value for the free carboxylate ion is usually taken as that of the sodium salt υ_{asym}(sodium acetate) = 1578 cm^{-1}.

Caution has to be taken in the analyses of the carboxylate stretching modes, since proper assignments can only be made when the oxidation state of manganese ions is taken into account.[51] FTIR data reported for a range of six-coordinate Mn complexes, i.e., with a di-$\mu_{1,3}$-acetato−Mn(II)OHMn(II), a di-$\mu_{1,3}$-acetato−Mn(III)OMn(III), and a di-$\mu_{1,3}$-acetato−Mn(III)-OMn(IV) core and Me_3TACN ligands, showed[52−54] that the asymmetric stretch of the bridging acetates shifts to lower energies upon conversion from Mn_2(II,II) to Mn_2(III,III) by 66 cm^{-1} (from 1636 to 1570 cm^{-1}) and Mn_2(III,IV) by 96 cm^{-1} (from 1636 to 1540 cm^{-1}). The data described above for complex **1** and its oxidized Mn_2(III,III) analogue display an opposite trend, i.e., a shift of the asymmetric stretch toward higher energy upon formation of the Mn_2(III,III) dimer, which therefore indeed indicates a change in the coordination mode to monodentate.[51] The same trend was observed for complexes **2**−**4** and their oxidized analogues; i.e., the unsymmetrical carboxylate stretch increases from 1596 to 1629 (complex **2)**), 1564 to 1632 (complex **3**) and 1592 to 1624 cm^{-1} (complex **4**). Because of overlap with modes from the benzimidazole ligand, it was impossible to clearly identify the symmetrical carboxylate stretch.

In contrast to the Mn_2(II,II) complexes, the spectra of the precipitated Mn_2(III,III) derivatives of complexes **1**−**4** all show a new absorption in the lower energy region between 583 and 590 cm^{-1}. In analogy with published data for other μ-oxo−Mn_2(III,III) complexes[49,55] this new band is tentatively assigned to a υ_{sym}(Mn−O−Mn) stretch. The υ_{asym}(Mn−O−Mn) stretch, which is expected around 720−750 cm^{-1}, could not be clearly resolved possibly because of overlap with a strong ligand-based absorption around 740−760 cm^{-1}, which is present for all of the complexes **1**−**4)**.

Mass Spectrometry. FAB and electrospray mass spectrometry measurements were used to monitor the changes induced by the addition of NaOH to complexes **1** and **3**. The FAB mass spectrum of complex **1** (given in Supporting Information, Figure S5) shows positive ion peaks correlating to **1**−$HClO_4$ (877, 30% rel intens), **1**−$HCLO_4$−HAc (817, 66% rel intens), and **1**−2HC-lO_4 (777, 100% rel intens) fragments. After oxidation to Mn_2-(III,III) by addition of NaOH (1−4 equiv) to a methanol solution of complex **1**, the FAB mass spectra (Supporting Information, Figure S5) show diminished intensities of the preceding peaks and two additional signals at 931 and 831 mass units, which correspond respectively to $\{[L^1Mn_2(III,III)(\mu\text{-}O)](ClO_4)_2\}^{1+}$ and $\{[L^1Mn_2(III,III)(\mu\text{-}O)](ClO_4)\}^{2+}$. The relative intensities of the molecular fragments corresponding to the original Mn_2(II,II) complex *decrease*, while the peaks corresponding to the oxidized species *increase* with each added equivalent of NaOH between 1 and 4 equiv, in full support of these assignments.

Measurements using a FAB ionization source are generally not quantitative, and interference with the matrix (thioglycerol in our case) can never be excluded. Therefore, the same experiment was done using an electrospray ionization source, which does not require the use of a supporting matrix. We did not observe ionization of complexes **1** and **2** with the electrospray source, but complexes **3** and **4** showed well-resolved and interpretable spectra. The electrospray mass spectrum of complex **3** shows a main signal at 989 *m*/*z* units (Supporting Information, Figure S6) corresponding to $\{[L^2Mn_2(II,II)(\mu\text{-}OAc)](ClO_4)\}^{1+}$. Upon addition of 1− 4 equiv of NaOH to a methanol solution of **3** the peak at 989 decreases in intensity, while two new molecular fragments appear, at *m*/*z* 1048 and 949, corresponding to the oxidized fragments $\{[L^2Mn_2(III,III)(\mu\text{-}O)](ClO_4)_2\}^{1+}$ and $\{[L^2Mn_2(III,III)(\mu\text{-}O)](ClO_4)\}^{2+}$ (Supporting Information, Figure S6).

While these experiments prove the formation of a Mn_2(III,III)−μ-oxo complex, neither the FAB nor electrospray experiments could we observe molecular fragments for an oxidized Mn_2(III,III) complex with a bound acetate. By contrast, both reduced Mn_2(II,II) complexes **1** and **3** could be ionized intact with bound acetate (bridging bidentate in this case). Thus, we conclude from MS data that the acetate is either not bound or weakly bound and dissociates from the Mn_2(III,III) complexes under the MS conditions used for ionization and/or volatilization in the gas phase. This result is consistent with the solution NMR

(50) Deacon, G. B.; Phillips, R. J. *Coord. Chem. Rev.* **1980**, *33*, 227.
(51) Smith, J. C.; Gonzales-Vergara, E.; Vincent, J. B. *Inorg. Chim. Acta* **1997**, *255*, 99.
(52) Wieghardt, K.; Bossek, U.; Nuber, B.; Weiss, J.; Bonvoisin, J.; Corbella, M.; Vitols, S. E.; Girerd, J. J. *J. Am. Chem. Soc.* **1988**, *110*, 7398.
(53) Wieghardt, K.; Bossek, U.; Ventur, D.; Weiss, J. *J. Chem. Soc., Chem. Commun.* **1985**, 347.
(54) Wieghardt, K.; Bossek, U.; Bonvoisin, J.; Beauvillain, P.; Girerd, J. J.; Nuber, B.; Weiss, J. *Angew. Chem., Int. Ed. Engl.* **1986**, *25*, 1030.
(55) Meesuk, L.; Jayasooriya, U. A.; Cannon, R. D. *J. Am. Chem. Soc.* **1987**, *109*, 2007.

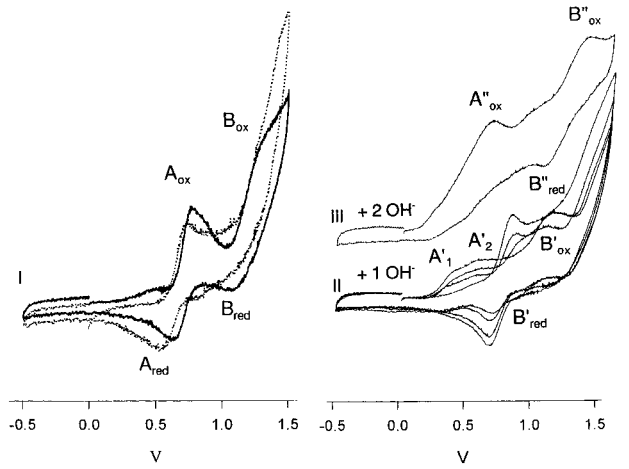

Figure 7. Cyclic voltammograms of complex **1** in acetone/TBAP solution (A), upon addition of 1 equiv NaOH (B), upon addition of 2 equiv of NaOH (C), and upon subsequent addition of 2 equiv of $HClO_4$ to (C), giving (D). The scan rate is 20 mV s^{-1}. See Table 2 and Scheme 1 for summary of electrochemical data.

data, which indicates a monodentate-coordinated acetate in equilibrium with free acetate for the oxidized Mn_2(III,III) species, obtained upon addition of more than 2 equiv of NaOH to **3** and **4**. However, while we do observe a μ_{13}-bridging acetate species, $[L^2Mn_2(III,III)(\mu\text{-O})(\mu\text{-OAc})]^{2+}$, in solutions by NMR upon addition of less than 2 equiv of NaOD to **3** and **4**, we do not observe this acetate species (MW = 1106 for L^2) under mass spectrometry conditions. This discrepancy could be due to an unfavorable ionization profile for $[L^2Mn_2(III,III)(\mu\text{-O})(\mu\text{-OAc})]^{2+}$ or instability of the product preventing it from detection. All structural assignments given in Scheme 3 are supported by solution NMR data, MS data, or both.

Electrochemistry. Several reports have dealt with protonation of μ-oxo bridges of dinuclear ruthenium, iron, and manganese complexes in solution.[18,52,56−62] The coupling of electron- and proton-transfer steps involving the $Mn_2(\mu\text{-O})_2^{n+}$ cores reveals that protonation of the μ-oxo leads to a substantial increase in the reduction potential of Mn_2 complexes, in many cases equal to the increase observed upon successive oxidation. Less data have been presented on the influence of protonation/deprotonation of nonbridging, nitrogen-containing ligands on the redox properties of metal complexes.[56,63,6463,64] This phenomenon is expected to be of major importance in nature because of the numerous examples of ionizable histidine ligands coordinating to metal sites in enzymes.

Figure 7I (solid line) shows a typical CV of complex **1** in acetone/TBAP. The initial oxidation at 790 mV, which is associated with a reduction at 700 mV (redox couple A), is assigned to a two-electron process on the basis of analogous results reported earlier in acetonitrile and by comparison to the peak current for a one-electron standard (ferrocene).[12,22] The quasi-reversibility of redox couple A is established by the linear relation between the current and the square root of the scan rate (not shown), indicating reversible or quasi-reversible electron transfer. This process is followed by an oxidation process at 1310 mV, which is associated with a reduction at 1190 mV (redox couple B). Redox couple B is assigned to be a one-electron process on the basis of analogous results obtained earlier in acetonitrile/TBAP showing also formation of a Mn_2(III,IV) EPR signal (net $3e^-$ oxidation of **1**.[12,41] All electrochemical data are summarized in Table 2.

Table 2. Summary of Electrochemical Data for Complex **1** Depicted in Figures 7 and 8 and Schemes 1 and 2

species	redox couple	E_{ox} (mV)	E_{red} (mV)	$E_{1/2}$ (mV)	no. e^-
1	A[a]	790	700	745	2
1 + 1OH^-	A_1'	350			1
1 + 1OH^-	A_2'	500			1
1 + 2OH^-	A″	600			2
1	B[a]	1310	1190	1250	1
1 + 1OH^-	B′	1060	910	985	1
1 + 2OH^-	B′	1290	1030	1160	2
1 + 1TBP	C	1040	910	980	1
1 + 2TBP	D[b]	∼1400			1

[a] Values in acetone/TBAP solution. In CH_3CN/TBAP values are the following: (couple A) $E_{1/2}$ is 690 mV; (couple B) $E_{1/2}$ is 1220 mV. [b] Value close to the solvent window and therefore less accurate.

1. Coordinating Base (OH^-). After titratration of an acetone/TBAP solution of complex **1** with 0.25, 0.5, and 1.0 equiv of NaOH, the subsequent CV waveforms (Figure 7II) show a decrease in the intensity of the original redox couples A and B of complex **1** and a proportional appearance of three new redox waves. Since the experiments were done under exclusion of oxygen, the bulk of complex **1** in solution remains in the reduced Mn_2(II,II) state. The new species shows two broad, partly overlapping, irreversible oxidation waves at, respectively, 350 mV (A'_1) and 500 mV (A'_2), a quasi-reversible redox couple with an oxidation wave at 1060 mV, and a corresponding reduction wave at 910 mV ($E_{1/2}$ is 980 mV, B′). This result indicates that upon binding of 1 equiv of hydroxide, the original two-electron oxidation of Mn_2(II,II), yielding Mn_2(III,III) at 790 mV (couple A), is now converted into two one-electron oxidation steps that are shifted to more reducing potentials by 440 (A'_1) and 290 mV (A'_2), respectively. Similarly, the one-electron oxidation of Mn_2(III,III) to Mn_2(III,IV) is shifted by 265 mV to more negative potential. The conversion of the two-electron equipotential (II,II ↔ III,III) oxidation to two one-electron oxidation steps (II,II ↔ II,III ↔ III,III) suggests the conversion of two independent redox centers to a more strongly interacting dinuclear Mn complex. The latter behavior is analogous to that observed with the μ-chloro- and μ-hydroxo-bridged species, $[L^1Mn(II,II)_2Cl_3]$ and $[L^1Mn_2(II,II)(\mu\text{-OH})Br_2]$, respectively, whose electrochemistry as shown before exhibits resolved one-electron oxidation processes.[14] Thus, the electrochemical data are in accord with the structural data given above, indicating that binding of the first equivalent of hydroxide to **1** at a bridging site between the two Mn(II) ions stabilizes the oxidized states and results in resolved one-electron redox transitions. This stabilization is attributed to stronger shielding of the intermanganese Coulomb coupling by μ-hydroxide. The magnitude of the difference in free energies ($\Delta\Delta G°/F = n\Delta E°$) for the two-electron-oxidized state with Mn_2(III,III) caused by addition of the μ-OH^- is proportional to the difference in the $2e^-$ potentials (Table 2): 1580 − 350 − 500 = 730 mV. The corresponding magnitude of the stabilization of the one-electron-

(56) Caroll, J. M.; Norton, J. R. *J. Am. Chem. Soc.* **1992**, *114*, 8788.
(57) Manchanda, R.; Thorp, H. H.; Brudvig, G. W.; Crabtree, R. H. *Inorg. Chem.* **1991**, *30*, 494.
(58) Manchanda, R.; Thorp, H. H.; Brudvig, G. W.; Crabtree, R. H. *Inorg. Chem.* **1992**, *31*, 4040.
(59) Manchandra, R.; Brudvig, G. W.; Crabtree, R. H. *Coord. Chem. Rev.* **1995**, *144*, 1.
(60) Kelson, E. P.; Henling, L. M.; Schaefer, W. P.; Labinger, J. A.; Bercaw, J. E. *Inorg. Chem.* **1993**, *32*, 2863.
(61) Geilenkirchen, A.; Neubold, P.; Schneider, R.; Wieghardt, K.; Florte, U.; Haupt, H. J.; Nuber, B. *J. Chem. Soc., Dalton Trans.* **1994**, 457.
(62) Hartman, J. R.; Rardin, R. L.; Chauduri, P.; Pohl, K.; Wieghardt, K.; Nuber, B.; Weiss, J.; Papaefthymiou, G. C.; Frankel, R. B.; Lippard, S. J. *J. Am. Chem. Soc.* **1987**, *109*, 9.
(63) Haga, M. *Inor. Chim. Acta* **1983**, *75*, 29.
(64) Sundberg, R. J.; Martin, R. B. *Chem. Rev.* **1974**, *74*, 471.

oxidized mixed-valence state Mn_2(II,III) caused by binding of the μ-OH ligand is proportional to the difference in the $1e^-$ potentials: 790 − 350 = 430 mV). In Scheme 1 these electrochemical data are plotted as a free energy diagram. Solid lines correspond to reversible redox couples, while the white bars correspond to the less accurate values for the irreversible couples. The stabilization in free energy upon binding of hydroxide to complex **1** is $-RT \ln K_{stab}$ in which the equilibrium constant K_{stab} corresponding to the reaction

$$\mathrm{OH^-} + \mathbf{1} \rightarrow \mathbf{1}\text{-OH}$$

is unknown, and therefore, the decrease in free energy for this conversion is chosen arbitrarily in Scheme 1 (symbolized as ? over each reaction).

Upon binding of a second equivalent of hydroxide, the two oxidation waves A'_1 and A'_2 merge and shift again to become one irreversible two-electron oxidation wave at a higher potential of 600 mV (Figure 7III, A''_{ox}; no reduction wave is observed). This behavior indicates that the two Mn(II) ions have become electronically decoupled again, making a two-electron equipotential oxidation favored. As depicted in Scheme 1, this result can be explained by the idea that binding of the second hydroxide causes displacement of the bridging hydroxide to a terminal position, yielding a symmetrical μ_{13}-acetato-di-μ-hydroxodimanganese(II,II) complex possessing two terminally coordinated hydroxides. This species is predicted to have a longer intermanganese separation than the mono-μ-hydroxo species and comparable or longer than the 3.54 Å Mn−Mn separation in precursor **1**. Addition of the second hydroxide is also observed to shift the oxidation wave B′ by 230 mV positive from 1060 to 1290 mV and increases the peak current by 2-fold (B''_{ox}, Figure 7III). This quasi-reversible oxidation wave B_{ox}'' is associated with a new reduction wave at 1030 mV (B_{red}''). On the basis of the shift in potential and the intensity of the current, we suggest that this new couple should represents a two-electron oxidation of Mn_2(III,III) → Mn_2(IV,IV), process B″ in Scheme 1.

Extensive electrolysis of a 1 mM acetone/TBAP solution of complex **1** with 2 equiv of NaOH at 1400 mV vs SCE leads to complete conversion with formation of a red-purple solution. This solution has a different λ_{max} = 490 nm and ϵ_{max} = 330 compared to the Mn_2(III,III) species produced in basic solution by autoxidation under air. EPR analysis of this solution shows that the majority of the generated species is EPR-silent and probably diamagnetic (estimated diamagnetic fraction of >95%), while a small quantity (<5%) of the previously characterized[41] mixed-valence Mn_2(II,III) derivative of **1** is observed. A diamagnetic EPR-silent species is expected for a magnetically coupled Mn_2(IV,IV) complex, although the absence of an EPR signal is insufficient evidence to be sure of this oxidation state.

Upon addition of more than 2 equiv of hydroxide a small oxidation wave at 150 mV arises that can be attributed to oxidation of uncoordinated NaOH (confirmed by addition of NaOH to an acetone/TBAP solution without **1**). No further changes in the redox processes of **1** are observed with addition of more than 2 equiv hydroxide. The changes noted above in the electrochemistry are reversible upon addition of equal amounts of perchloric acid (Figure 7I, dotted line); i.e., the successive redox couples A and B reappear except that they are slightly shifted toward more reducing potentials (40 and 60 mV, respectively, for couples A and B). This small shift might be caused by the presence of water or by a different coordination mode of the acetate group after treatment of **1** with water (hydroxide and perchloric acid), as was discussed above for the hydrolysis reaction monitored by NMR spectroscopy (Scheme 3, step A).

2. N-Alkyl Derivatives. The observed stabilization of the higher oxidation states of **1** upon addition of base can also be expected in principle if deprotonation of the NH groups of the coordinated benzimidazoles were to occur. To distinguish between hydroxide coordination and ligand deprotonation, the electrochemistry of complex **3**, in which the benzimidazole nitrogens are alkylated, was also studied. The electrochemistry of complex **3** is very similar to the electrochemistry of the nonethylated complex **1** in acetonitrile/TBAP. Two quasi-reversible couples can be observed at 690 and 1220 mV vs SCE. By contrast to complex **1**, complex **3** is very insoluble in acetone/TBAP. Therefore, a voltammogram of **3** itself could not be obtained in acetone. By addition of 1 equiv of hydroxide to complex **3** in acetone/TBAP a part of the complex solubilizes (while remaining colorless under an argon atmosphere) and the voltammogram shows two oxidation waves at 500 (broad) and 910 mV, analogous to processes A'_{1+2} and B′, respectively. Although the absolute values of the redox couples for complex **3** + 1 equiv of NaOH are different from the redox couples for complex **1** + 1 equiv of NaOH, the observed trend, i.e., stabilization of the high-valent Mn(III,III), (III,IV), and (IV,-IV) species, is the same for both complexes. We observe from this experiment that the effect of hydroxide on the electrochemistry of both complexes is essentially identical and therefore conclude that it cannot be due to deprotonation of the benzimidazole NH protons.

3. Benzimidazoyl Deprotonation. A new reaction can be observed when a stereochemically encumbered noncoordinating base such as 2,6-di(t-butyl)pyridine (TBP) is used instead of hydroxide. In this case deprotonation of the benzimidazole groups of the ligand L^1 occurs (Scheme 2). The pK_a of free benzimidazole ligand has been reported to be 5.5 (in water) and 12.3 (in acetonitrile). Because of binding of the benzimidazole-containing ligand (L^1) to manganese, the pK_a of the benzimidazole proton will decrease. The amount of the decrease is dependent on the oxidation state of the manganese. Upon addition of small (0.2−1.0 equivalent) aliquots of TBP to complex **1** in acetonitrile/TBAP solution a third (quasi-)-reversible transition (C) appears in the voltammogram at $E_{1/2}$ = 980 mV (E_{ox} is 1050 mV; E_{red} is 910 mV) as illustrated in Figure 8. The appearance of couple C is proportional to the disappearance of couple B upon successive additions of 0.0, 0.2, and 0.6 equiv TBP to **1** (Figure 8). After the addition of more than 0.6 equiv of TBP, both couples C and B increase in intensity because of overlap with a new oxidation wave D, an irreversible transition at 1400 mV. Because D occurs close to the limit of the solvent window, it is difficult to analyze. However, the current for process D increases further upon addition of more (1.0−4.0 equiv) TBP. No change is observed in couple A throughout the titration with TBP (Figure 8). The redox couples A, B, and C show a linear relation between the current and the square root of the scan rate, indicating reversible or quasi-reversible electron transfer. The TBP-induced transformations are completely reversible upon addition of the corresponding equivalents of $HClO_4$, which restores the original voltammogram (not shown). All necessary blanks were done to ensure that the new transitions do not originate from TBP itself or its protonated form, free ligand, or deprotonated free ligand.

We interpret these results according to Scheme 2 in which one benzimidazoyl group on the ligand L^1 is deprotonated by 1

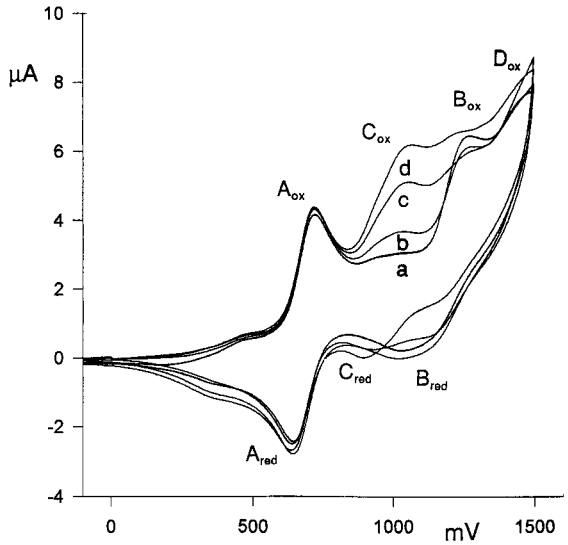

Figure 8. Cyclic voltammograms of complex **1** in acetonitrile/TBAP solution upon addition of (a) 0, (b) 0.2, (c) 0.6, and (d) 1.0 equiv of TBP to deprotonate the benzimidazoyl nitrogens. The scan rate is 50 mV s^{-1}. See Table 2 and Scheme 2 for summary of electrochemical data.

equiv TBP, forming L^1-H, but only after complex **1** is first oxidized (step A) to the Mn_2(III,III) state. Following this deprotonation step, the second oxidation process (step C) forms the mixed-valence $(L^1-H)Mn_2$(III,IV) species, which is stabilized by an additional 150 mV relative to the original (III,IV) species, couple B. The appearance of a new oxidation process at 1.4 V (step D) upon further addition of 1−4 equiv TBP is proposed to be due to removal of a second benzimidazoyl proton yielding L^1-2H and resulting in one-electron oxidation of $(L^1-2H)Mn_2$(III,IV) to $(L^1-2H)Mn_2$(IV,IV).

In Scheme 2 the electrochemical data are plotted as a free energy diagram. The free energy changes for the proton ionization steps, labeled ΔG_1 and ΔG_2 in this scheme, were not measured and so are shown only qualitatively. However, we know that there is a lower limit for ΔG_1 in the first ionization step that is bounded by the pK_a of TBP at $\Delta G_1 > (2.3RT)$pK_a, on the basis of the observation that TBP does not affect the potential for the initial oxidation process, step A. The pK_a of TBP is 4.95 in water[65] but has not been reported in acetonitrile. A relationship between the pK_a values in aqueous media and acetonitrile has been developed:[66] pK_a(CH_3CN) = pK_a(H_2O) + 7.5. Therefore, a lower limit for ΔG_1 was calculated to be 14.3 kJ using a pK_a of 12.5 for TBP in acetonitrile.

Upon addition of TBP to the acetonitrile/TBAP solution containing the N-ethylated complex **3**, no changes in the electrochemistry are observed. This result proves that TBP acts to deprotonate the benzimidazoyl protons of the ligand in complex **1**, in contrast to OH^-, which acts as a ligand to the Mn ions.

General Discussion and Conclusion

We have summarized the observed reactions of the dimanganese(II,II) complex **1** and its analogues (**2**−**4**) in Scheme 3. Upon addition of water to a dry methanol or acetone solution of complex **1** (step A, Scheme 3), less than 20% of the spin-coupled Mn_2(II,II) dimer is converted to a spin-uncoupled species, as indicated by EPR results. We attribute this conversion to the reversible hydrolysis of complex **1** to form species **5A** or **5B**, in which the μ-alkoxide bridge is broken by protonation and the resulting hydroxide binds to Mn(II). EPR spectroscopy established that this reaction can be reversed by addition of 1 equiv of hydroxide, which restores the spin-coupled Mn_2(II,II) species. An analogous "alkoxide shift" reaction has been proposed before[67] in the homolytic cleavage of alkyl hydroperoxides by Mn_2(III,III) $(2\text{-OHsalpn})_2$, generating a free site on one of the manganese ions necessary for the substrate to coordinate.

On the basis of electrochemical results, we conclude that addition of 1 equiv of hydroxide to a dry solution of **1**−**4** (step B, Scheme 3) produces a species in which the hydroxide ligand bridges between the two Mn ions, resulting in a strongly coupled Mn_2(II,II)(μ-OH) dimer (**7A**) possessing an EPR-silent ground state. In this hydroxo-bridged dimer the Mn_2(II,III), Mn_2(III,-III), and Mn_2(III,IV) oxidation states are stabilized by 440, 290, and 230 mV, respectively, compared to the original Mn_2(II,II) complex **1**. Subsequent addition of air (step C, Scheme 3), leads to oxidation of Mn_2(II,II) to Mn_2(III,III) (**8**), as was shown by EPR, optical absorption, EI-MS, and NMR. The most compelling evidence for the structure of **8** comes from ^{1}H NMR measurements. Both of the Mn_2(III,III) derivatives **8A** and **8B)** obtained from the complexes **3** and **4**, respectively, were shown by NMR to be strongly antiferromagnetically coupled and to have a symmetrically bridging alkoxide of the chelate ligand (L^1 and L^2, respectively) and a nonlabile $\mu_{1,3}$-bridging acetate, as was shown by electrochemistry, FTIR, and mass spectrometry. NMR measurements established the conversion of the tightly bound $\mu_{1,3}$-acetate into a loosely bound monodentate acetate ligand upon addition of 1−2 equiv of NaOH to complex **8** (step D, Scheme 3), yielding complex **6**. Complex **6** was isolated as a pure solid and characterized by NMR, FTIR, UV−vis spectroscopy, EI-MS, and electrochemistry.

The interconversion between bidentate and monodentate geometries of carboxylate ligands (so-called "carboxylate-shift"[68]) on binuclear complexes is of importance because it allows expansion of the coordination sphere in cases where substrate binding is coupled to redox cycling of the metal center (as, for example, in the hydrogen peroxide disproportionation reaction). Furthermore, it has been proposed that bridging carboxylates may serve a functional role beyond that of a passive structural bridge, i.e., that their size and negative charge enable them to spatially separate and Coulombically screen the electropositive metal ions so that the direct intermetallic interaction is small. This screening results in both Mn(II) ions undergoing oxidation at close to the same oxidation potential in a simultaneous two-electron process.[69] If the redox potential is tuned to the same or lower reduction potential as the peroxide dismutation reaction, this two-electron redox couple can then be used for catalysis. The superexchange part of the intermanganese interaction represents an insignificant contribution to the energy of interaction in carboxylate-bridged Mn_2(II,II) complexes[44] but may contribute a small term relative to the Coulombic term in Mn_2(III,III) complexes. As is shown here (Scheme 1, step B), this screening and separation function of

(65) Hopkins, H. P.; Jahagirdar, D. V.; Moulik, P. S.; Aue, D. H.; Webb, H. M.; Davidson, W. R.; Pedley, M. D. *J. Am. Chem. Soc.* **1984**, *106*, 4341.
(66) Kristjansdottir, S. S.; Norton, J. R. In *Transition Metal Hydrides: Recent Advances in Theory and Experiment*; Dedieu, A., Ed.; VCH: New York, 1992; p 309.
(67) Caudle, M. T.; Riggs-Gelasco, P.; Gelasco, A. K.; Penner-Hahn, J. E.; Pecoraro, V. L. *Inorg. Chem.* **1996**, *35*, 3577.
(68) Rardin, R. L.; Tolman, W. B.; Lippard, S. J. *New. J. Chem.* **1991**, *15*, 417.
(69) Dismukes, G. C. Manganese Enzymes with Binuclear Active Sites. *Chem. Rev.* **1996**, *96*, 2909.

the bridging carboxylates can be greatly suppressed by addition of a bridging hydroxide ion, which again increases the intermetallic coupling and decreases the metal ion separation. The effect on the free energy is quite dramatic, as shown in Scheme 1. Formation of the μ-OH^- species (**7**) by addition of one OH^- to complexes **1**−**4** makes removal of the first electron easier by 440 mV. In marked contrast, addition of the second OH^- leads to a higher oxidation potential (vs μ-OH) by 250 mV, which can be attributed to breaking of the μ-OH^- bridge to form the di-OH^--mono-$\mu_{1,3}$-acetato derivative. As can be seen in Scheme 1, for complex **1** with two coordinated hydroxides it is energetically more favorable by 36.6 kJ ($\Delta\Delta G^\circ = -nF\Delta E^\circ$ for $n = 2$ and $\Delta E^\circ = 190$ mV) to undergo a single two-electron oxidation step than without coordinated hydroxides and more favorable by 79.4 kJ when there is one bridging μ-OH^-. Thus, it is clear in comparing the potentials that the bridging position for the hydroxide ligand provides a substantially greater stabilization of the two-electron-oxidized Mn_2(III,III) state. The same argument holds true for stabilization of the one-electron-oxidized Mn_2(II,III) state. When compared to both the hydroxide-free derivatives and the terminal bishydroxide derivatives, the energy of stabilization for μ-OH^--bridging coordination of Mn_2 species is 42.4 kJ (440 mV) and 18.3 kJ (250 mV), respectively, for the Mn_2(II,III) state, and 79.4 kJ (730 mV) and 35.1 kJ (350 mV), respectively, for the Mn_2(III,III) state (Table 2 and Scheme 1).

The results also show that by reaction of the Mn_2(II,II) complexes **1**−**4** with 1 or >3 equiv of hydroxide under air, it is possible to generate two types of Mn_2(III,III) complexes, LMn_2(III,III)(μ-O)(μ-Oac) (**8**) and LMn_2(III,III)(μ-O)(OH)(Oac) (**6**), respectively. NMR spectroscopy readily distinguishes these two forms.

Equipped with these new derivatives, we examine in the next paper[42] their kinetic properties for disproportionation of H_2O_2. Predictions can be made based on the physicochemical properties that are reported in this paper. The reduction of the redox gap between the Mn_2(II,II) and Mn_2(III,III) oxidation states is thought to be important for controlling the catalase rate, since the rate-determining step is oxidation of the Mn_2(II,II) center.[12] Closing this energy gap by ligand deprotonation with a noncoordinating base, like TBP, proved to be impossible for the Mn_2(II,II)/Mn_2(III,III) couple because TBP is not able to deprotonate the benzimidazoyl ligand in complexe **1** or **2** and not in the Mn_2(II,II) or the Mn_2(III,III) oxidation states, as is summarized in Scheme 2. One may expect that inhibition of catalase activity should occur upon formation of the Mn_2(III,IV) state on the basis of the observed behavior for the enzymes.[9,69,70] Therefore, it could be expected that the addition of TBP should produce no substantial change in the catalase rate via the two-electron pathway involving the Mn_2(II,II)/(III,III) couple, assuming that the activation barrier is determined by this redox potential. If, however, the Mn_2(III,IV) oxidation state is involved in catalase activity, the addition of TBP should accelerate the disproportionation rate, since TBP does deprotonate the benzimidazoyl ligand in this oxidation state and substantially lowers the energy gap for the Mn_2(III,III)/(III,IV) couple (Scheme 2).

By contrast, if the II,II/III,III redox couple were the only factor controlling the catalase rate, addition of one OH^- should, on one hand, increase the rate, since the potential for the μ-OH^- bridged species is considerably reduced. On the other hand, the original two-electron oxidation step is now converted into two one-electron steps by binding of μ-OH^-, which might lead to the production of catalytically inactive mixed-valence species. Addition of the second hydroxyl ion displaces the μ-OH^- to a terminal site, forming the dihydroxo species Mn_2(II,II)$(OH)_2$, and restores the two-electron couple A″ for Mn_2(II,II)/(III,III)-$(OH)_2$, which has a potential only 190 mV lower than that of the hydroxide-free derivative. Thus, thermodynamically one expects that the catalase rate should increase for Mn_2(II,II)-$(OH)_2$ both because the potential is more favorable than for the original complex **1** and because there are two intramolecular hydroxides to serve as Bronsted bases for deprotonation of the H_2O_2 substrate during oxidation to O_2. We examine all of these factors in the following paper.[42]

Acknowledgment. We express our gratitude to Profs. G. McLendon and A. Bocarsly for access to voltammetry instrumentation and Dr. G. Ananyev for technical assistance. The research is supported by U.S. National Institutes of General Medical Sciences (GM39932). A.E.M.B. acknowledges a fellowship from The Netherlands Organization for Scientific Research.

Supporting Information Available: Figures showing optical, NMR, EPR, and MS data for various compounds. This material is available free of charge via the Internet at http://pubs.acs.org.

IC9911769

(70) Waldo, G. S.; Penner-Hahn, J. E. *Biochemistry* **1995**, *34*, 1507.